Desalination and Water Treatment
www.deswater.com
doi: 10.1080/19443994.2015.1108871

57 (2016) 20552–20564
September

Taylor & Francis
Taylor & Francis Group

Comparative study of dye degradation using TiO_2-activated carbon nanocomposites as catalysts in photocatalytic, sonocatalytic, and photosonocatalytic reactor

Pardeep Singh[a], M.C. Vishnu[b], Karan Kumar Sharma[b], Rishikesh Singh[c], Sughosh Madhav[d], Dhanesh Tiwary[a], Pradeep Kumar Mishra[b,*]

[a]*Department of Chemistry, Indian Institute of Technology (BHU), Varanasi 221005, India, emails: psingh.rs.apc@itbhu.ac.in (P. Singh), dtiwari.apc@itbhu.ac.in (D. Tiwary)*
[b]*Department of Chemical Engineering and Technology, Indian Institute of Technology (BHU), Varanasi 221005, India, Tel./Fax: +91 05426702036; email: vishnu.mc.che12@itbhu.ac.in (M.C. Vishnu), karan.ksharma.che12@itbhu.ac.in (K.K. Sharma)*
[c]*Institute of Environment & Sustainable Development (IESD), Banaras Hindu University (BHU), Varanasi 221005, India, email: rishikesh.iesd@gmail.com*
[d]*School of Environmental Sciences, Jawaharlal Nehru University (JNU), New Delhi 110067, India, email: sughosh.madhav@gmail.com*

Received 3 February 2015; Accepted 8 October 2015

ABSTRACT

In the present study, activated carbon-based TiO_2 nanocomposites with carbon loading were synthesized by sol–gel method for photocatalytic, sonocatalytic, and sonophotocatalytic degradation of colored compound in wastewater. The prepared catalysts were characterized by Brunauer–Emmet–Teller surface area analysis, X-ray diffraction (XRD), scanning electron microscopy (SEM), and Fourier transform infrared analysis (FT-IR). The degradation efficiencies of the synthesized composites were determined by the degradation of Direct Blue-199 dye under three different reactors viz., photocatalytic, sonocatalytic, and sonophotocatalytic. Reaction kinetic modeling was done for these processes and the degradation rate was found maximum for sonophotocatalytic process as compared to individual ones. However, on considering the energy efficiency and degradation efficiency, photochemical reactor was found to be most economical. Therefore, for the treatment of wastewater-containing dye from industries, a photocatalytic process can be applied with further modification.

Keywords: Activated carbon TiO_2; Nanocomposites; Synthetic dye; Photocatalytic; Sonocatalytic; Sonophotocatalytic; Reaction kinetics; Energy efficiency

1. Introduction

Numerous dyes are extensively consumed in various textile and fabric industries for products coloration because of their property of persisting long-term intense exposure to sunlight and other environmental effects. More than 100,000 dyes are being used for industrial purposes, a considerable amount of which after processing is released out along with the effluents, polluting soil, and water resources [1,2]. The

*Corresponding author.

diversity in the chemical composition of the synthetic dyes makes them impervious to color fading [3]. Among these dyes, basic and azo direct dyes are considered to have soaring toxicity issues [4]. Direct blue 199, utilized for various purposes, has high visibility in water even at low concentration which impedes sunlight and affects photosynthesis. Being carcinogenic, its discoloration from the industrial effluent should be prioritized [5].

Various conventional techniques being practiced for dye discoloration have both favorable as well as disadvantageous issues regarding time, cost, and byproducts [6]. Further because of the presence of aromatic compounds and stability of the synthetic dye, these methods are ineffective for discoloration and mineralization [7]. They transfer the pollutants to other phase, rather than destroying them or produce secondary pollutants [8,9]. Advanced oxidation processes and their combinations such as ultrasound (US) [10] and ozonation (O_3) [11], TiO_2 [12], ultraviolet (UV) [13], H_2O_2 [14], and Fenton reagent [15] are impactful treatment methods. Application of ultrasonic irradiation in core experiments has been appreciated for its effectiveness in degrading the recalcitrant pollutants such as dyes [16]. Ultrasound waves, generated in this process causes homolytic cleavage of the H_2O within cavitation bubbles, producing $OH^{\cdot}$ and $H^{\cdot}$ [6,17]. Where upon the degradation of the pollutants in aqueous solution is carried by these free radicals. Hazardous dye pollutants in effluent require complete mineralization (conversion into H_2O, CO_2 and mineral acids) for safer disposal. However, this mineralization does not approach an appreciable extent due to several factors like hydrophilic intermediate products and reaction volume [18,19].

Recently, degradation of pollutants by photocatalyst-based processes has been reported in many literatures [20–23]. Among effective semiconductors, TiO_2 has been widely utilized as a photocatalyst due to its strong oxidizing power, low cost, and non-carcinogenic nature [24]. However, its low efficiency when used in pristine form is due to low ratio of light utilization, difficulty in separation form bulk solution, etc. [25]. Further, the electrons and holes formed upon impact of irradiation recombine which further adds to its limitation [26]. These hindrances can be overcome by adsorbing TiO_2 particles on carbonaceous adsorbents having large surface area such as activated carbon (AC) [27]. AC is a good support for semiconductor for photocatalytic activity because it acts as electron carrier to inhibit the recombination of electron–hole pair and provides large contact area as well as additional surface pH for enhanced photocatalytic activity [28]. In general, the production of TiO_2/AC nanocomposite is cheaper, viable, and reproducible as per industrial requirements, when compared to other processes. Further, degradation of dye by the TiO_2/AC composite has been appreciated as a reliable industrial process. However, the use of traditional UV sources causes a high heat dissipation which results in high energy cost and also requires an additional cooling mechanism in the reactor. Recently, various studies were conducted on the feasibility of the UV Light Emitting Diodes as a light source of photocatalytic degradation of organic pollutants [29–31].

The rudimentary reason behind the mechanism of degradation by both photocatalysis and sonolysis is the generation of $OH^{\cdot}$ radical. Both processes involve the mineralization of dyes into simpler molecules of H_2O, CO_2, etc. Hence, the combined effect of both processes i.e. sonophotocatalysis allows a greater impact on the degradation of these pollutants, though it involves more power consumption when compared to individual processes. Sonophotocatalysis creates a synergic effect between both of its rudimentary processes [32]. Recent studies have shown that TiO_2/AC nanocomposite enhances the oxidative activity of ultrasonic waves even in the absence of ultraviolet irradiation [33]. The presence of this catalyst during ultrasonication enhances the formation of acoustic cavitation bubbles whose explosion generates $OH^{\cdot}$ radical and hence supports the alleviated degradation process [34].

Present study involves comparison of photocatalysis, sonolysis, and sonophotcatalysis processes for Direct Blue 199 dye degradation. AC using rice husk was prepared and used for the preparation of TiO_2/AC nanocomposite by sol gel method calcined at two different temperatures. An elaborate reaction kinetics study for each process was done and the rate constants were compared. As the dye's removal from effluent is a serious concern, the power consumption of all three processes is compared to highlight their cost effectiveness, taking into account the kinetic study of the processes considering the viability and cost-promising factors.

2. Materials and method

2.1. Source of dye

Direct Blue 199 Dye was brought from Sigma-Aldrich (CAS no. 4399-55-7) with empirical formula is $C_{40}H_{28}N_7NaO_{13}S_4$ (Hill notation) and molecular weight 965.94 (approx.)

2.2. Preparation of photo-catalyst

TiO_2 loaded on activated charcoal (AC/TiO_2) was used as the catalyst for the process. Activated charcoal

was prepared from rice husk obtained from the nearby rice mill, by treating the husk with concentrated H_2SO_4 in the weight ratio (1:1) at 150˚C in an oven for 24 h. The mixture was then cooled and the excess acid present in the material was leached out by washing with (1% w/v) sodium bicarbonate solution and followed by washing with distilled water. The mixture was then finely ground to 200 mesh after drying [35].

Then sol–gel method was used to prepare AC/TiO_2 catalyst [36–38]. Titanium tetra- isopropoxide (TTIP) was used as a binder. During the preparation process, 35.8 gm of TTIP was dissolved in 180 ml of 99.9% propanol and 20 ml of 34% HCl (w/v) and the mixture was kept in a reciprocating shaker for 1 h (h) for homogenization. The resulting solution was diluted to 1,000 ml by adjusting pH (3) by adding NaOH, 10 g of AC and 10 g of P25 TiO_2 particles were mixed together and stirred for 3 h. Obtained gel solution was then filtered through membrane filter and oven-dried at 80˚C for 24 h. The dried samples were crushed and calcinated at different temperatures, viz., 350 and 450˚C for 3 h. The final ratio of TiO_2 particles to AC in the catalyst was 1.99 (w/w). AC/TiO_2 catalyst was then used in the further processes.

2.3. Design of reactors

Three reactors were used during the experiments. A photochemical reactor which consisted of a cylindrical reactor fitted in with 8 Phillips UV lamps of intensity 8 W along with a magnetic stirrer. Similarly, to carry out sonication reaction, another reactor was fitted with a Sonicator (Hielsher Ultrasound Technology) instead of UV lamps. Finally, a reactor consisting of a combined photo- and sonocatalytic mechanism was also set up as shown in (Fig. 1). All these reactors were provided with cooling jackets with water flowing inside them so as to avoid overheating.

Various solutions consisting of different concentrations of dye, along AC/TiO_2 catalyst were used for the experiments. The experiments were conducted in the three different reactors. The samples were taken out from the batch reactor at fixed time interval and their concentration was measured. This data were then used for further deductions and calculations.

3. Results and discussion

3.1. Characterization of catalyst

3.1.1. Brunauer Emmet Teller surface area analysis

Specific surface area (SSA) of samples of AC/TiO_2 nanocomposites was assayed using Brunauer–Emmet–Teller plot with relative pressure (p/p_0) ranging from 0.01 to 0.20 [39]. The sample calcined at the temperature of 250˚C has a SSA of 201.35 m^2/gm. When compared to sample being calcined at higher temperature of 350˚C whose SSA is 288.70 m^2/gm. Therefore, the heat treatment temperature has large effect on the activity of AC/TiO_2 nanocomposites by changing its SSA, crystallinity, carbon residual, etc. [40,41].

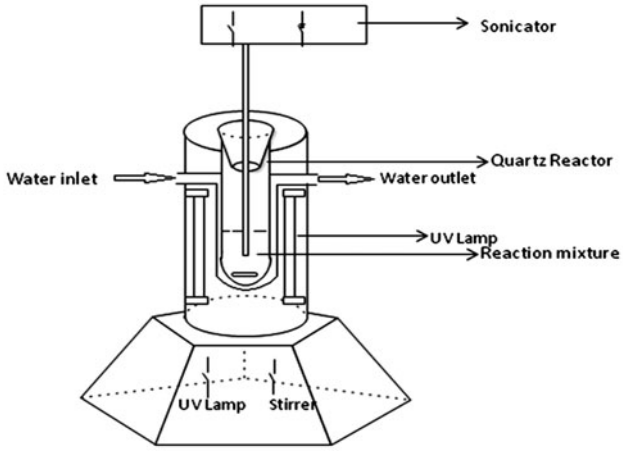

Fig. 1. Schematic diagram of the sonophotocatalytic reactor.

3.1.2. X-ray diffraction (XRD) analysis

X-ray diffraction analysis was performed to assay the phase composition and crystalline nature and size of prepared AC/TiO_2 nanocomposites were used to identify the peaks of the sample by comparing with the standard data. Various diffraction peaks as shown in (Fig. 2) at $2\theta = 25.4^\circ$, 48.02°, 54.19°, and 62.72° were given by AC/TiO_2 nanocomposite which were assigned to (1 0 1), (2 0 0), (1 0 5), and (1 0 3) reflections of anatase phase and peaks at $2\theta = 37.80^\circ$ being assigned to (2 1 0) reflect the rutile phase of TiO_2. The average intensity of rutile phase is considerably less as compared to that of anatase phase. Scherrer's equation can be used to determine the average crystalline size Eq. (1) [42].

$$D = \frac{k\lambda}{\beta \cos \theta} \quad (1)$$

where k = Scherer constant, λ = X-ray wavelength and β = the peak width of half maximum and θ = Bragg diffraction angle.

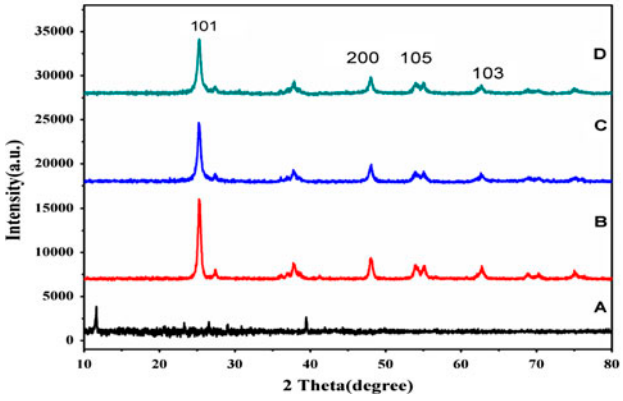

Fig. 2. XRD spectra of (A) activated carbon, (B) TiO_2, (C) AC/TiO_2 calcined at 250°C and (D) AC/TiO_2 calcined at 350°C.

3.1.3. Scanning electron microscope analysis

The TiO_2/AC nanocomposite was observed in scanning electron microscope for investigating its surface characterization and structure. TiO_2 particle was clearly observed as well dispersed and intertwined on AC. The surface morphology of TiO_2/AC nanocomposites was obtained as shown in (Fig. 3).

3.1.4. FTIR analysis

FTIR spectra of AC/TiO_2-nanocomposite give the number of peaks at different wave number (Fig. 4). Peak at 3,415 cm^{-1} represents the stretching of hydroxyl (O–H) group in water as moisture [43]. Peak at 1,614 cm^{-1} shows the stretching of titanium carboxylate, which was the product of TTIP and ethanol used in sol gel method. Calcination of TiO_2 at higher temperature removes the hydroxyl and carboxylate peaks. Peak at 667 cm^{-1} represents the stretching of Ti–O bond which is the characteristic attribute of the formation of TiO_2 nanoparticles. In addition, the hydroxyl group is not visible in AC's spectra [44]. FTIR study of AC/TiO_2 nanoparticles shows the shift in the OH vibration band toward lower wave number (3,400 cm^{-1}) when compared to that corresponding to TiO_2. These shifts confirm the alteration of acid–base characteristics of OH group in the used samples. The bands below 1,000 cm^{-1} represent Ti–O–C, indicating a weak conjugation between Ti–O bonds and AC [45]. The peaks obtained in the Fourier transform infrared analysis (FT-IR) spectra of catalysts prior and after the degradation were almost similar (as shown in Fig. 4).

3.2. Optimization of catalyst

Two photocatalysts were prepared by calcinating at two different temperatures, viz., 350 and 250°C. Thereafter, a plot between concentration and time for a given sample of DB-199 was made. It could be easily inferred that catalyst calcined at 350°C was more effective (as shown in Fig. 5) for a given set of reaction conditions under constant UV irradiation. This is due to the fact that at higher temperatures, the crystallinity is improved and hence, increasing the photocatalytic activity [46].

3.3. UV–vis spectrum analysis of the dye

The maximum absorbance values were determined by scanning absorbencies in 200–800 nm wavelengths using a Systronics' UV Spectrophotometer. The maximum absorbance peak between 200 and 400 nm shows the aromatic content in the dyes, while the peaks obtained in the range of 400–800 nm show the absorption in the visible range [47,48]. This spectrum analysis result was used in determining the wavelength (λ = 635.4 nm) for optical density measurement.

3.4. Photocatalytic, sonocatalytic and sonophotocatalytic decolorization of dyes: mathematical modeling and reaction kinetics

3.4.1. Photocatalytic decolorization of Direct Blue-199 (DB-199)

The reaction of DB-199 in presence of AC/TiO_2 nanocomposite and UV irradiation is an example of heterogeneous catalysis. Rate laws in such reactions seldom follow proper law models and hence are inherently more difficult to formulate from the data. It has been widely accepted that heterogeneous catalytic reactions can be analyzed with the help of Langmuir–Hinshelwood (LH) Model [43–49], with the following assumptions being satisfied, (i) there are limited number of adsorption sites on the catalyst and its surface is homogeneous, (ii) only one molecule can be adsorbed on one site and monolayer formation occurs (as in chemisorptions), (iii) the absorption reaction is reversible in nature, and (iv) The adsorbed molecules do not react amongst themselves [49–52]. According to LH Model, following steps take place in the kinetics mechanism [53–55].

Step 1

$$D\ (\text{Dye}) + C\ (\text{catalyst}) \leftrightarrow D.C$$

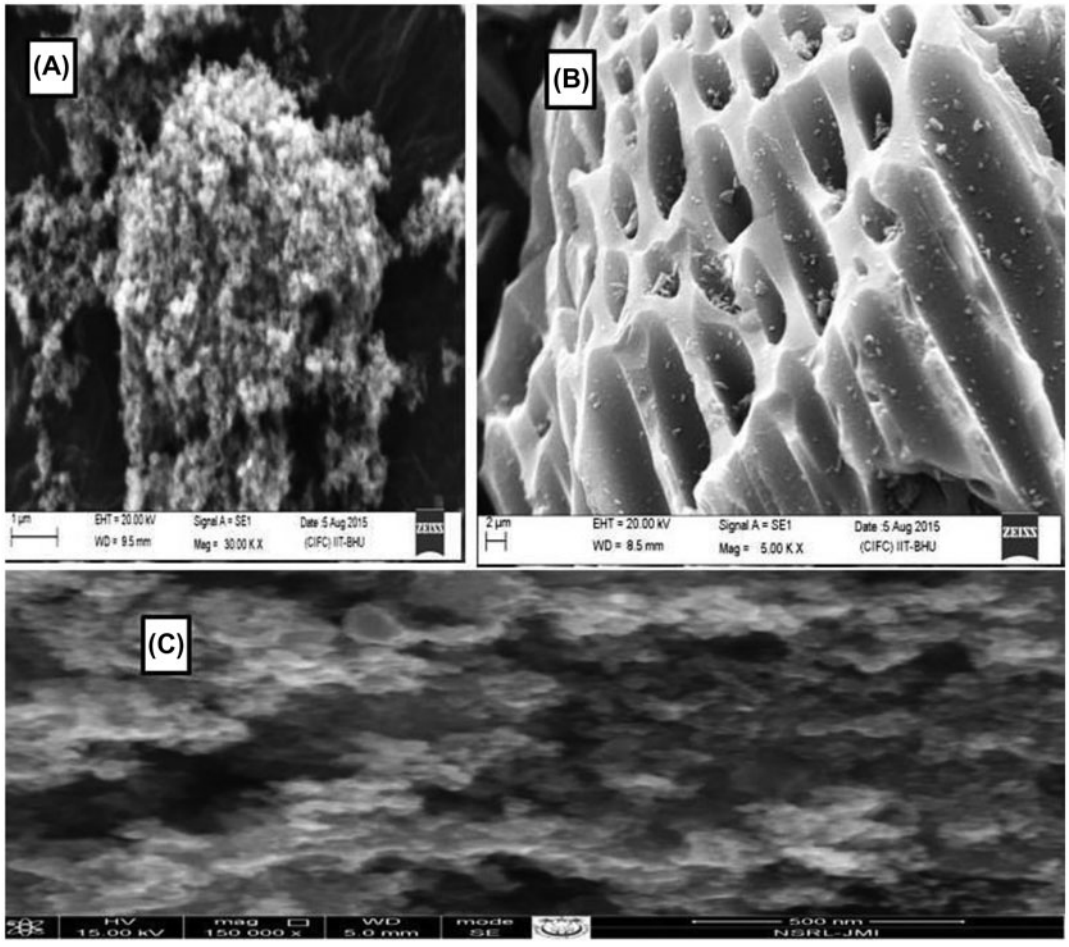

Fig. 3. SEM image (A) TiO_2, (B) activated carbon, and (C) AC/TiO_2 composite.

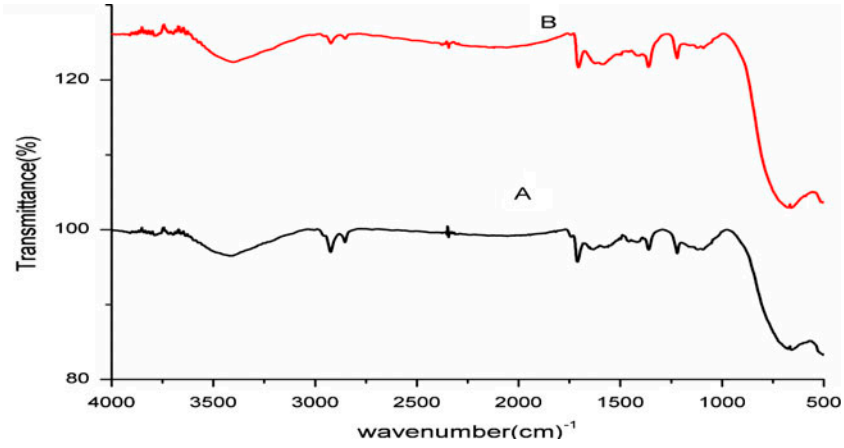

Fig. 4. FT-IR spectra of TiO_2/AC nanocomposite (A) after degradation and (B) before degradation of dye.

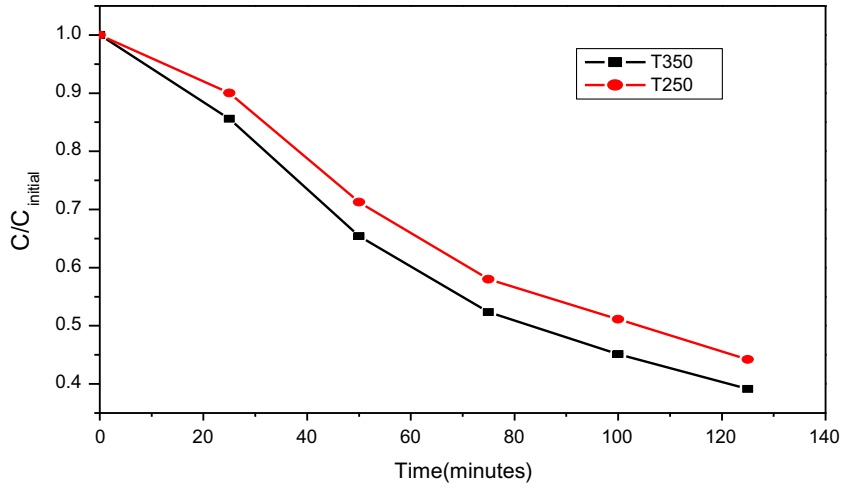

Fig. 5. Graph showing the change in concentration vs. time at two different calcination temperatures of the catalyst (250 and 350°C).

Adsorption of dye onto the catalyst surface.

Step 2

$D.C \leftrightarrow E.C + \text{Other products}$

Surface reaction

Step 3

$E.C \leftrightarrow E + C$

Desorption of products from the surface.

A control experiment was first carried out under two conditions, vis (i) dye + UV (no TiO_2) (ii) TiO_2 + dye in dark without any irradiation (Fig. 6). It can be seen that under dark conditions, after 25 min the amount of catalyst adsorbed becomes constant i.e. equilibrium adsorption is achieved. For the kinetic study of bleaching of DB-199, the initial concentration of the dyes was varied and the experiments were first conducted in dark for 25 min and then immediately followed by UV irradiation (Fig. 7). The amount of catalyst was kept constant (0.5 gm/L) throughout the experiment.

3.4.1.1. Absorption of dye onto the catalyst. Since the TiO_2 will be covered by both DB-199 (C) as well as water molecules (C_{water}) by hydrogen bonding, their competition for the active sites cannot be ignored. Langmuir's adsorption model can be applied to the aqueous solutions of dyes with the help of the following expression:

$$\theta = \frac{D_t}{D_{max}} = \frac{K_A C}{1 + K_A C + K_{water} C_{water}} \tag{2.1}$$

where θ is the fractional sites covered by the dye, D_t is the absorbed quantity of dye at any time, D_{max} shows the maximum quantity of dye that can be adsorbed, K_A is the Langmuir adsorption constant for reactant, K_{water} is the adsorption constant for water. The value of $C_{water} >> C$, hence C_{water} remains almost same throughout the reaction and the catalyst coverage by water molecules remains almost constant. Thus, we can ignore the quantity K_{water}, C_{water} and rewrite Eq. (2.1) as:

$$\theta = \frac{K_A C}{1 + K_A C} \tag{2.2}$$

The quantity adsorbed at a particular time can also be expressed as:

$$D_t = \frac{(\text{Reactor volume}) \times (\text{Change in concentration})}{\text{Mass of catalyst}} \tag{3}$$

The equilibrium adsorption quantity D_{eq} can be written as:

$$D_{eq} = D_{max}\left[\frac{K_A C_{eq}}{1 + K_A C_{eq}}\right] \tag{4}$$

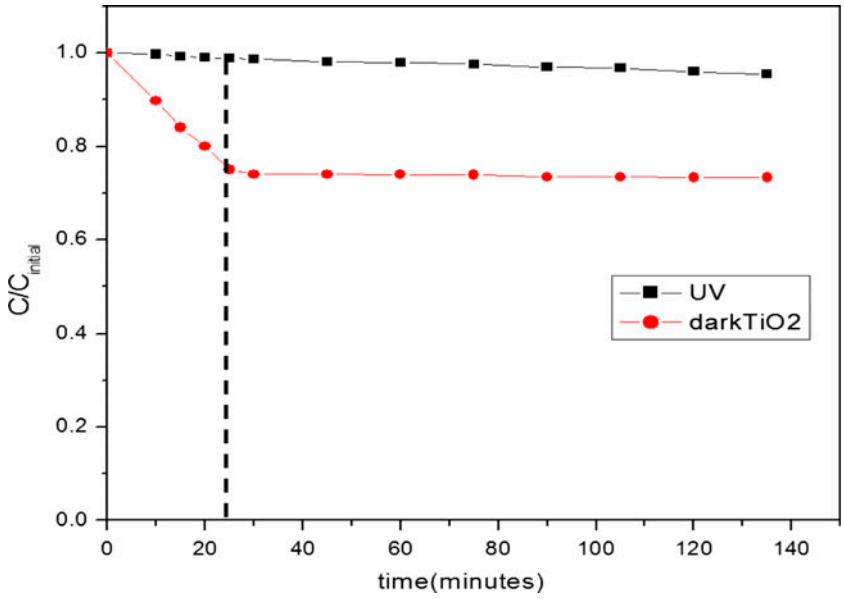

Fig. 6. Plot of change in concentration vs. time for (i) dye + UV, (ii) TiO_2 + dye in dark.

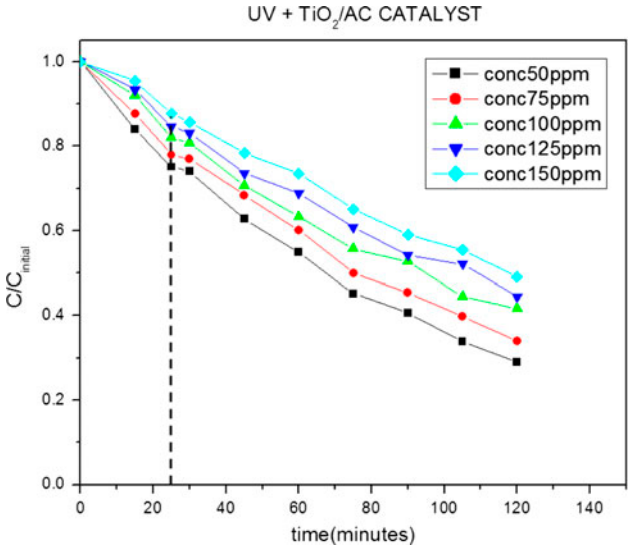

Fig. 7. Change in concentration of dye vs. time in presence of UV and AC/TiO_2 (the initial concentrations were 50, 75, 100, 125, and 150 ppm).

where C_{eq} is the equilibrium concentration of the dye. On transforming Eq. (4), a function can be derived as follows: $C_{eq}/D_{eq} = f(C_{eq})$

$$\frac{C_{eq}}{D_{eq}} = \frac{1}{K_A D_{max}} + \frac{C_{eq}}{D_{max}} \quad (5)$$

From (Fig. 8) the intercept on the vertical axis gives $1/K_A D_{max}$ and the reciprocal of slope gives D_{max}. The obtained parameters were tabulated as shown in Table 1.

3.4.1.2. Photocatalytic degradation. Applying the Langmuir–Hinshelwood model for determining the oxidation rate of the photocatalysis of dye:

$$\text{Rate } (r) = -\frac{dC}{dt} = k\theta = \theta = \frac{kK_A C}{1 + K_A C} \quad (6)$$

where k is the rate constant (mg/L min), C is the concentration of dye, K_A is the adsorption constant of the dye (L/mg), and t is the illumination time (min).

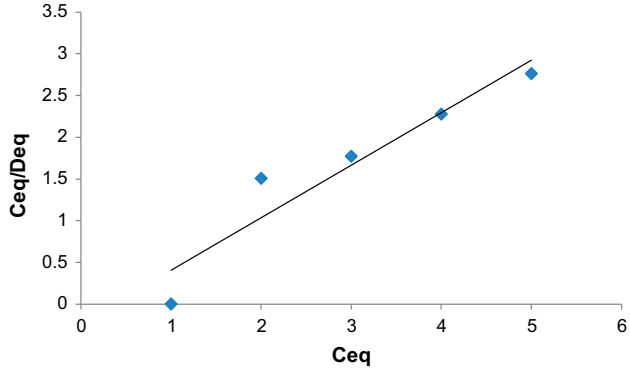

Fig. 8. Plot of ratio of equilibrium concentration to equilibrium adsorption quantity vs. equilibrium concentration representing a straight line.

Table 1
The parameters of adsorption characteristics of DB-199: K_A (Langmuir constant), D_{max} (maximum adsorbable quantity)

Parameter	Value
K_A (L/mg)	0.03856
D_{max} (mg of dye/gm of catalyst)	45.8715
R^2	0.9796

During the course of reaction, the initial pH, amount of catalyst, and photointensity were kept same. In addition to it, the formation of intermediates may interfere in the rate determination, hence the calculations were done at the beginning of UV irradiation. The rate expression can be written as:

$$r_o = \frac{kK_AC_o}{1 + K_AC_o} \tag{7}$$

where r_o is the initial rate of degradation of DB-199, C_o is the initial concentration (almost equal to C_{eq}). When the initial concentration $C_{initial}$ is very small, C_o will also be small and Eq. (7) can be simplified as an first-order equation [46–49,51]:

$$-\frac{dC}{dt} = kK_AC_o \equiv \ln\left(\frac{C_o}{C}\right) = kK_At \tag{8}$$

$$C = C_oe^{-k_{f,photo}t}$$

where

$$k_{f,photo} = kK_A \tag{9}$$

The value of $k_{f,photo}$ can be determined from the plot of $\ln(C_o/C)$ vs. t. The slope of the straight line obtained will be the value of first-order rate constant. Table 2 shows the values of apparent rate constant for DB-199 degradation.

Obtaining a linear transformation from Eq. (7), we get $1/r_o = f(1/C_o)$

$$\frac{1}{r_o} = \frac{1}{k} + \frac{1}{kK_AC_o} \tag{10}$$

$$\text{Also } r_o = k_fC_o \tag{11}$$

Using Eqs. (10) and (11) a linear regression of $1/r_o$ vs. $1/C_o$ was carried out and also a curve of r_o (initial rate) vs. C_o (initial concentration) was made (Figs. 9 and 10). It can be clearly seen that initial rate of the reaction increases with an increase in the increase initial concentration. Also the linear plot of $1/r_o$ vs.

Table 2
Value of apparent rate constant at various initial concentrations of dye solution for photocatalysis reaction

$C_{initial}$ (mg/l)	k_f (min^{-1})	R^2
50	0.01001	0.9809
75	0.00876	0.9760
100	0.00712	0.9805
125	0.00623	0.9913
150	0.00512	0.9645

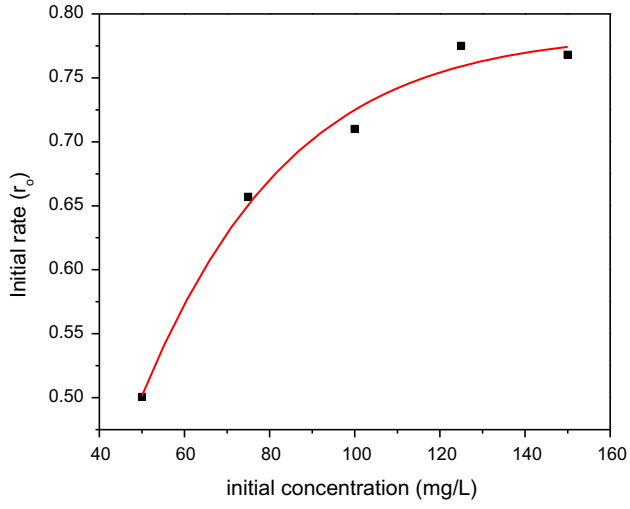

Fig. 9. Plot showing initial rate (r_o) vs. concentration of dye (C_o).

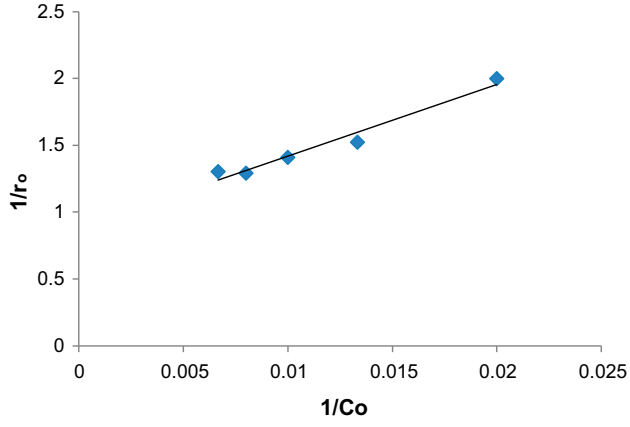

Fig. 10. Plot showing the linear variation of reciprocal of initial rates vs. reciprocal of initial concentration.

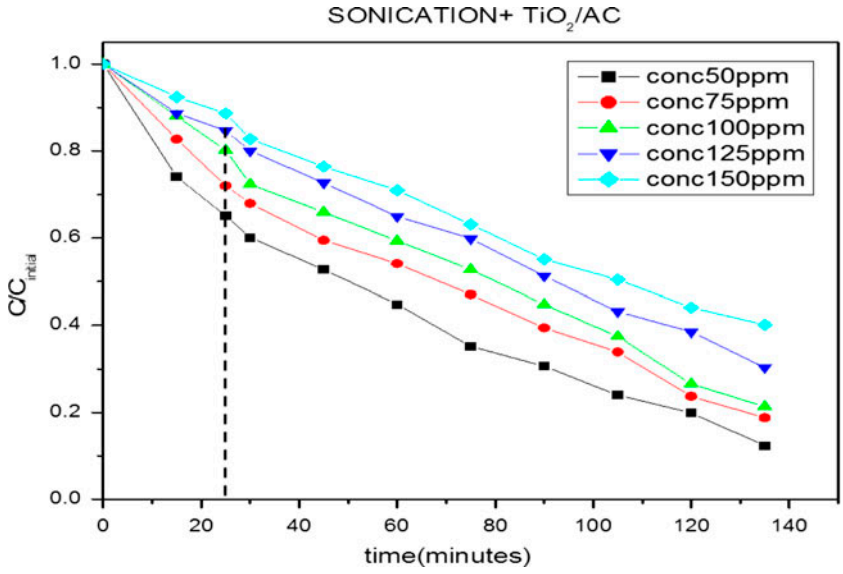

Fig. 11. Change in concentration of dye vs. time with sonication and AC/TiO_2 (the initial concentrations were 50, 75, 100, 125, and 150 ppm).

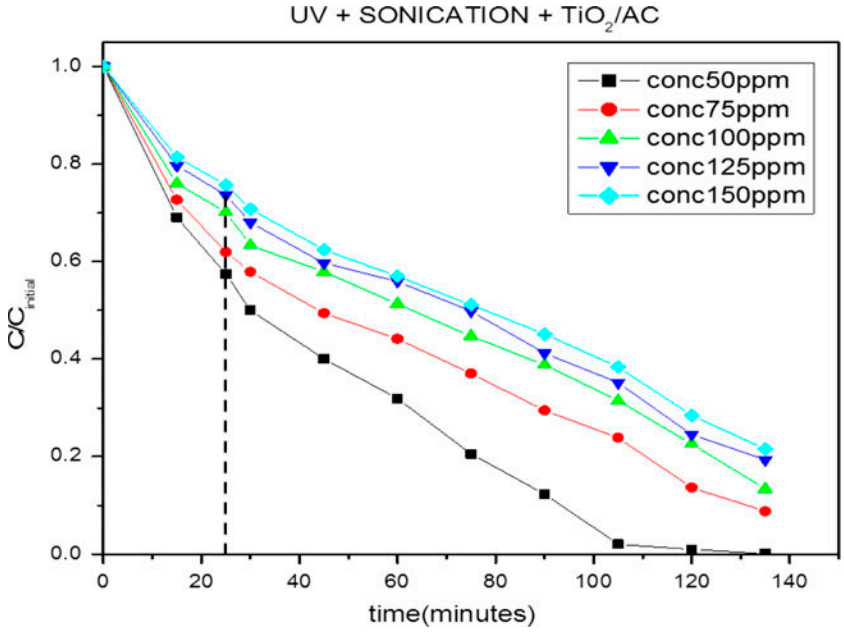

Fig. 12. Change in concentration of dye vs. time in presence of UV, sonication and AC/TiO_2 (the initial concentrations were 50, 75, 100, 125, and 150 ppm).

$1/C_o$ shows that L–H model is satisfied by the reaction. Thus, it can be said that in photocatalytic degradation of dye, initially adsorption of dye takes place and then degradation reaction (surface reaction) occurs.

The values of k and K_A obtained (from slope and intercept) were 1.135 min^{-1} and 0.016 L/mg, respectively. The value of K_A obtained from adsorption isotherm was not equal to K_A obtained from the L–H model. Ideally, $[K_A]_{L-H} = [K_A]_{adsorption}$, but in this case

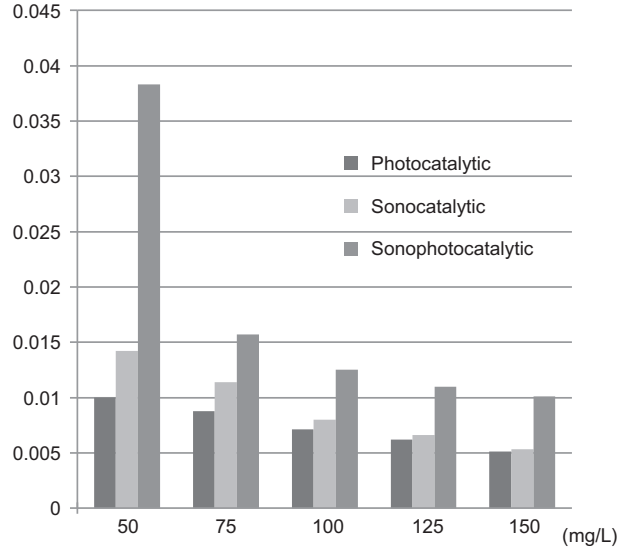

Fig. 13. Histogram showing the apparent first order rate constants for the three reactors.

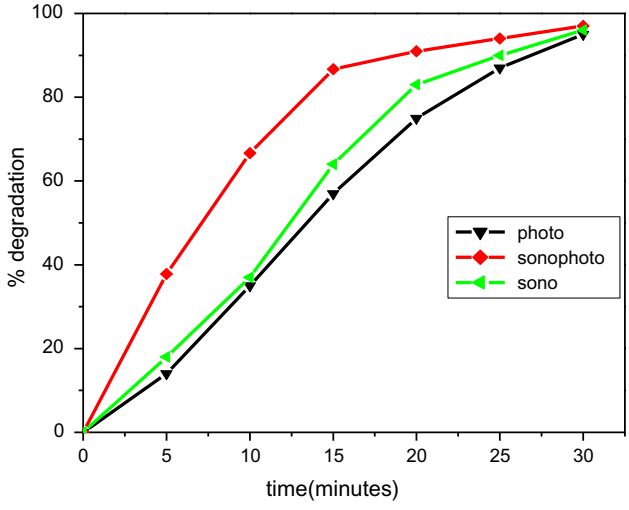

Fig. 14. Degradation (%) vs. time for the photocatalytic, sonocatalytic and sonophotocatalytic reactors.

$[K_A]_{L-H} = 0.414[K_A]_{adsorption}$. Various explanations have been attributed to this: (i) adsorption occurs at the surface as well as in the bulk of the solution, (ii) non-homogeneity of the adsorption sites, (iii) adsorption of more than one molecule at one adsorption site, and (iv) deficiency of adsorption sites [43,46,47].

3.4.2. Sonocatalytic and sonophotocatalytic decolorization of Direct Blue-199 (DB-199)

The change in concentration vs. time study was done for the other two reactors too vis. sonocatalytic and sonophotocatalytic as shown in (Figs. 11 and 12). The amount of catalyst taken was same as that for the photocatalysis reaction i.e. 0.5 gm/L.

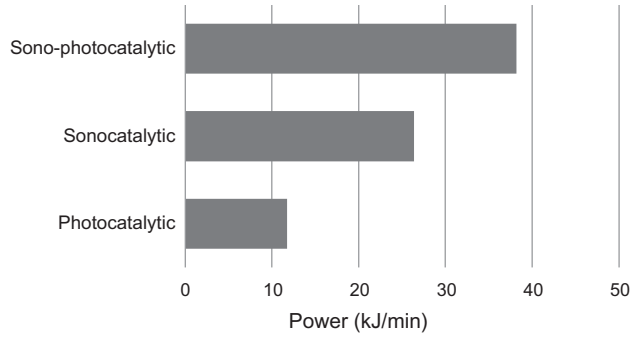

Fig. 15. Graph showing the power consumption by photo-catalytic, sonocatalytic and photo- and sonocatalytic reactor.

Both these reactions were assumed to follow the Langmuir–Hinshelwood Model. The value of k_f (apparent I order rate constant) for each process was calculated using Eqs. (12) and (13) (at different concentration of dye).

$$\ln\left(\frac{C_o}{C}\right) = k_{f,sono}t \tag{12}$$

$$\ln\left(\frac{C_o}{C}\right) = k_{f,sonophoto}t \tag{13}$$

where $k_{f,sono}$ and $k_{f,sonophoto}$ are apparent rate constants for sonocatalysis and sonophotocatalysis, respectively, and t is time in minutes.

A comparative study was done as shown in (Fig. 13). It can be seen clearly that rate constant of sonophotocatalysis which is the highest followed by sonocatalysis and photocatalysis being the least.

Thus, $k_{f,sonophoto} > k_{f,sono} > k_{f,photo}$

3.5. Efficiency of the reactors

Degradation comparison: to determine which of the aforementioned processes is the most efficient in terms of degradation efficiency, experiments were carried out at a fixed concentration of dye (100 mg/l). The reactions were conducted in the three reactors and the % degradation vs. time plot was drawn for each (as shown in (Fig. 14). The sonophoto catalytic reactor was the fastest to degrade the sample of dye. It was followed by sonocatalytic and photocatalytic reactors. However, higher degradation rate is not the only criteria for choosing the reactor, the energy consumed must also be considered.

Table 3
The amount of energy consumed, % degradation in 30 min and the overall reactor performance factor (*f*) by the various reactors

Type of reactor	Total energy consumed (kJ)	Degradation (%) (after 30 min)	$f = \frac{(\%\ \text{Degradation}) \times \text{time (min)}}{\text{Total energy consumed (kJ)}}$
Photocatalytic	348	92	7.93
Sonocatalytic	660	94	4.27
Sono-photocatalytic	763.2	98	3.85

3.5.1. Energy efficiency

The Perkit India's Photochemical Reactor (λ = 185 nm), consisting of 8 Phillips (TUV 8W T5 G8) mini lamps, with wattage 196 W was used. The sonocatalytic reactor (Hielsher Ultrasound Technology) had an power consumption of 440 J/s and frequency 26 kHz. The combined reactor (sono- and photocatalytic) operated at wattage of 636 W as shown in (Fig. 15). For the purpose of comparing, the each reactor's practical feasibility a reactor performance factor [*f*] was defined as shown in (Eq. (14)). This factor holistically comprises the % degradation, total time consumed in degradation and total energy consumption by the reactor.

$$f = \frac{(\%\ \text{Degradation}) \times \text{time}}{\text{Total energy consumed}} \tag{14}$$

On comparing the data in Table 3, the overall reactor performance factor was found to be highest for photocatalytic reactor with a value of 7.93. It can be attributed to the very low power consumption by photocatalytic reactor as compared to sonocatalytic and photosonocatalytic reactor. Thus, further work can be ensued upon to exploit the given reactor's degradation potential in wastewater treatment units, especially in those which treat wastewater-containing dye.

4. Conclusions

In this work, degradation analysis of DB-199 dye was done. A catalyst, TiO_2 loaded on activated charcoal, was prepared in the process and its characterizations showed an even distribution of TiO_2 on the catalyst's surface. The catalyst's calcinations temperature was also optimized and was found to be nearly ≈350 ℃. A first-order reaction kinetics was then developed for the catalytic oxidation of dye using L–H model. Following were the salient points of the experiments:

(1) The results suggested that degradation of DB-199, via photocatalytic, sonocatalytic and sonophotocatalytic reactions, under optimized working conditions followed L–H model satisfactorily.
(2) These three reactors used for the degradation of dye were tested on the basis of bleaching rates as well as energy consumption. Photocatalytic reactor was found to be the best option amongst the three reactors used.
(3) The contribution of intermediates formed during the reaction is not considered in the above kinetics study; however, there have been reports on competitive involvement of intermediate products during the photochemical process. Thus, for further development of reaction kinetics model, role of intermediates can be involved.

Symbols and Abbreviations

AC/TiO_2	—	TiO_2 loaded on activated charcoal
US	—	ultrasonication
UV	—	ultraviolet irradiation
θ	—	fractional sites covered by the dye over the catalyst
D_t	—	absorbed quantity of dye at a particular time
D_{max}	—	maximum quantity of dye that can be adsorbed
K_A	—	Langmuir Adsorption constant for reactant
K_{water}	—	adsorption constant for water
D_{eq}	—	equilibrium adsorption quantity
C_{eq}	—	equilibrium concentration of the dye
r_o	—	initial rate of reaction
r	—	rate of reaction at any concentration
$k_{f,photo}$	—	apparent first-order rate constant for photocatalytic reaction
$k_{f,sono}$	—	apparent first-order rate constant for sonocatalytic reaction
$k_{f,sonophoto}$	—	apparent first-order rate constant for sonophotocatalytic reaction
[*f*]	—	reactor performance Factor

References

[1] T. Robinson, G. McMullan, R. Marchant, P. Nigam, Remediation of dyes in textile effluent: A critical review on current treatment technologies with a proposed alternative, Bioresour. Technol. 77 (2001) 247–255.

[2] Ratna, B.S. Padhi, Pollution due to synthetic dyes toxicity & carcinogenicity studies and remediation, Int. J. Environ. Sci. 3 (2012) 940–955.

[3] V.J.P. Poots, G. McKay, J.J. Healy, The removal of acid dye from effluent using natural adsorbents—I peat, Water Res. 10 (1976) 1061–1066.

[4] J. Shore, Advances in direct dyes, Indian J. Fib. Text. Res. 21 (1996) 1–29.

[5] Y. Ding, C. Sun, X. Xu, Simultaneous identification of nine carcinogenic dyes from textiles by liquid chromatography/electrospray ionization mass spectrometry via negative/positive ion switching mode, Eur. J. Mass Spectrom. 15 (2009) 705–713.

[6] M. Kitajima, S. Hatanaka, S. Hayashi, Mechanism of O_2-accelerated sonolysis of bisphenol A, Ultrasonics 44 (2006) e371–e373.

[7] S. Tunesi, M.A. Anderson, Photocatalysis of 3,4-DCB in TiO_2 aqueous suspensions; effects of temperature and light intensity, CIR-FTIT interfacial analysis, Chemosphere 16 (1987) 1447–1456.

[8] V. Golob, A. Vinder, M. Simonic, Efficiency of the coagulation/flocculation method for the treatment of dyebath effluents, Dyes Pigm. 67 (2005) 93–97.

[9] C. Fersi, M. Dhahbi, Treatment of textile plant effluent by ultrafiltration and/or nanofiltration for water reuse, Desalination 222 (2008) 263–271.

[10] X. Zhou, W. Guo, S. Yang, H. Zheng, N. Ren, Ultrasonic-assisted ozone oxidation process of triphenylmethane dye degradation: Evidence for the promotion effects of ultrasonic on malachite green decolorization and degradation mechanism, Bioresour. Technol. 128 (2012) 827–830.

[11] I. Fuentes, J.L. Rodríguez, T. Poznyak, I. Chairez, Photocatalytic ozonation of terephthalic acid: A by-product-oriented decomposition study, Environ. Sci. Pollut. Res. 21 (2014) 12241–12248.

[12] R. Byberg, J. Cobb, L.D. Martin, R.W. Thompson, T.A. Camesano, O. Zahraa, M.N. Pons, Comparison of photocatalytic degradation of dyes in relation to their structure, Environ. Sci. Pollut. Res. 20 (2013) 3570–3581.

[13] Z. Zhang, Y. Yuan, G. Shi, Y. Fang, L. Liang, H. Ding, L. Jin, Photoelectrocatalytic activity of highly ordered TiO_2 nanotube arrays electrode for azo dye degradation, Environ. Sci. Technol. 41 (2007) 6259–6263.

[14] N.H. Ince, Critical effect of hydrogen peroxide in photochemical dye degradation, Water Res. 33 (1999) 1080–1084.

[15] P.V. Nidheesh, R. Gandhimathi, S.T. Ramesh, Degradation of dyes from aqueous solution by Fenton processes: A review, Environ. Sci. Pollut. Res. 20 (2013) 2099–2132.

[16] X.-J. Zhou, W.-Q. Guo, S.-S. Yang, H. Zheng, N.R. Key, Ultrasonic-assisted ozone oxidation process of triphenylmethane dye degradation: Evidence for the promotion effects of ultrasonic on malachite green decolorization and degradation mechanism, Bioresour. Technol. 128 (2013) 827–830.

[17] K.S. Suslick, Sonochemistry, Science 247 (1990) 1439–1445.

[18] J. Peller, O. Wiest, P.V. Kamat, Synergy of combining sonolysis and photocatalysis in the degradation and mineralization of chlorinated aromatic compounds, Environ. Sci. Technol. 37(9) (2003) 1926–1932.

[19] V. Ragaini, E. Selli, C.L. Letizia Bianchi, C. Pirola, Sono-photocatalytic degradation of 2-chlorophenol in water: Kinetic and energetic comparison with other techniques, Ultrason. Sonochem. 8 (2001) 251–258.

[20] P. Muthirulan, C.N. Devi, M.M. Sundaram, TiO_2 wrapped graphene as a high performance photocatalyst for acid orange 7 dye degradation under solar/UV light irradiations, Ceram. Int. 40(4) (2014) 5945–5957.

[21] M. Ahmad, E. Ahmed, Z.L. Hong, W. Ahmed, A. Elhissi, N.R. Khalid, Photocatalytic, sonocatalytic and sonophotocatalytic degradation of Rhodamine B using ZnO/CNTs composites photocatalysts, Ultrason. Sonochem. 21(2) (2014) 761–773.

[22] Priyanka, V.C. Srivastava, Photocatalytic oxidation of dye bearing wastewater by iron doped zinc oxide, Ind. Eng. Chem. Res. 52 (2013) 17790–17799.

[23] N. Khalfaoui-Boutoumi, H. Boutoumi, H. Khalaf, B. David, Synthesis and characterization of TiO_2–Montmorillonite/polythiophene-SDS nanocomposites: Application in the sonophotocatalytic degradation of rhodamine 6G, Appl. Clay Sci. 80–81 (2013) 56–62.

[24] M.M. Haque, M. Muneer, Photodegradation of norfloxacin in aqueous suspensions of titanium dioxide, J. Hazard. Mater. 145 (2007) 51–57.

[25] X. Wang, Z. Hu, Y. Chen, G. Zhao, Y. Liu, Z. Wen, A novel approach towards high-performance composite photocatalyst of TiO_2 deposited on activated carbon, Appl. Surf. Sci. 255 (2009) 3953–3958.

[26] J. Yu, Q. Xiang, M. Zhou, Preparation, characterization and visible-light-driven photocatalytic activity of Fe-doped titania nanorods and first-principles study for electronic structures, Appl. Catal. B: Environ. 90 (2009) 595–602.

[27] J. Matos, R. Montaña, E. Rivero, Influence of activated carbon upon the photocatalytic degradation of methylene blue under UV–vis irradiation, Environ. Sci. Pollut. Res. 22 (2015) 784–791.

[28] A. García, J. Matos, Photocatalytic activity of TiO_2 on activated carbon under visible light in the photodegradation of phenol, Open Mater. Sci. J. 4 (2010) 2–4.

[29] W.K. Jo, R.J. Tayade, Recent developments in photocatalytic dye degradation upon irradiation with energy-efficient light emitting diodes, Chin. J. Catal. 35 (2014) 1781–1792.

[30] W.K. Jo, G.T. Park, R.J. Tajade, Synergetic effect of adsorption on degradation of malachite green dye undee blue LED irradiation using spiral-shaped photocatalytic reactor, J. Chem. Technol. Biotechnol. 90 (2015) 2280–2289.

[31] K. Natarajan, T.S. Natarajan, H.C. Bajaj, R.J. Tayade, Photocatalytic reactor based on UV-LED/TiO_2 coated quartz tube for degradation of dyes, Chem. Eng. J. 178 (2011) 40–49.

[32] N. Talebian, M.R. Nilforoushan, F.J. Mogaddas, Comparative study on the sonophotocatalytic degradation of hazardous waste, Ceram. Int. 39 (2013) 4913–4921.

[33] Y. Wang, D. Zhao, W. Ma, C. Chen, J. Zhao, Enhanced sonocatalytic degradation of Azo Dyes by Au/TiO_2, Environ. Sci. Technol. 42 (2008) 6173–6178.
[34] M. Ahmad, E. Ahmed, Z.L. Hong, W. Ahmed, A. Elhissi, N.R. Khalid, Photocatalytic, sonocatalytic and sonophotocatalytic degradation of Rhodamine B using ZnO/CNTs composites photocatalysts, Ultrason. Sonochem. 21 (2014) 761–773.
[35] R.M. Suzuki, A.D. Andrade, J.C. Sousa, M.C. Rollemberg, Preparation and characterization of activated carbon from rice bran, Bioresour. Technol. 98 (2007) 1985–1991.
[36] H. Inoue, T. Matsuyama, B.J. Liu, T. Sakata, H. Mori, H. Yoneyama, Photocatalytic activities for carbon dioxide reduction of TiO_2 microcrystals prepared in SiO_2 matrices using a sol–gel method, Chem. Lett. 23 (1994) 653–656.
[37] Y. Horie, M. Taya, S. Tone, Effect of cell adsorption on photosterilization of *Escherichia coli* over titanium dioxide–activated charcoal granules, J. Chem. Eng. Jpn. 31 (1998) 922–929.
[38] M. Kubo, H. Fukuda, X.J. Chua, T. Yonemoto, Kinetics of ultrasonic degradation of phenol in the presence of composite particles of titanium dioxide and activated carbon, Ind. Eng. Chem. Res. 46 (2007) 699–704.
[39] S. Brunauer, P.H. Emmett, E. Teller, Adsorption of gases in multimolecular layers, J. Am. Chem. Soc. 60 (1938) 309–319.
[40] H. Wu, J. Ma, C. Zhang, H. He, Effect of TiO_2 calcination temperature on the photocatalytic oxidation of gaseous NH_3, J. Environ. Sci. 26 (2014) 673–682.
[41] J. Araña, J.M. Doña-Rodriguez, E.T. Rendón, C.G. Caḅo, O.G. Díaz, J.A.H. Melián, J. Pérez-Peña, G. Colón, J.A. Navio, TiO_2 activation by using activated carbon as a support Part I. Surface characterisation and decantability study, Appl. Catal. B: Environ. 44 (2003) 161–172.
[42] H. Borchert, E.V. Shevchenko, A. Robert, I. Mekis, A. Kornowski, G. Grübel, H. Weller, Determination of nanocrystal sizes: A comparison of TEM, SAXS, and XRD studies of highly monodisperse $CoPt_3$ particles, Langmuir 21 (2005) 1931–1936.
[43] M.M. Ba-Abbad, A.A.H. Kadhum, A.B. Mohamad, M.S. Takriff, K. Sopian, Synthesis and catalytic activity of TiO_2 nanoparticles for photochemical oxidation of concentrated chlorophenols under direct solar radiation, Int. J. Electrochem. Sci 7 (2012) 4871–4888.
[44] M. Hema, A.Y. Arasi, P. Tamilselvi, R. Anbarasan, Titania nanoparticles synthesized by sol–gel technique, Chem. Sci. Trans. 2 (2013) 239–245.
[45] B. Tryba, A.W. Morawski, M. Inagaki, A new route for preparation of TiO_2-mounted activated carbon, Appl. Catal. B: Environ. 46 (2003) 203–208.
[46] S. Yang, X. Yang, X. Shao, R. Niu, L. Wang, Activated carbon catalyzed persulfate oxidation of Azo dye acid orange 7 at ambient temperature, J. Hazard. Mater. 186 (2011) 659–666.
[47] H. Lachheb, E. Puzenat, A. Houas, M. Ksibi, E. Elaloui, C. Guillard, J.M. Herrmann, Photocatalytic degradation of various types of dyes (Alizarin S, Crocein Orange G, Methyl Red, Congo Red, Methylene Blue) in water by UV-irradiated titania, Appl. Catal. B: Environ. 39 (2002) 75–90.
[48] G.A. Epling, C. Lin, Photoassisted bleaching of dyes utilizing TiO_2 and visible light, Chemosphere 46 (2002) 561–570.
[49] R.W. Matthews, Kinetics of photocatalytic oxidation of organic solutes over titanium dioxide, J. Catal. 111 (1988) 264–272.
[50] M. Vautier, C. Guillard, J.M. Herrmann, Photocatalytic degradation of dyes in water: Case study of Indigo and of Indigo Carmine, J. Catal. 201 (2001) 46–59.
[51] J. Cunningham, G. Al-Sayyed, S. Srijaranai, Adsorption of model pollutants onto TiO_2 particles in relation to photoremediation of contamined water, in: G. Helz, R. Zepp, D. Crosby D., J. Photochem. Photobiol., A, Lewis Publs., CRC Press, Boca Raton, Florida, Chap., 22, 1994, pp. 317–348.
[52] E. Vulliet, J.M. Chovelon, C. Guillard, J.M. Herrmann, Factors influencing the photocatalytic degradation of sulfonylurea herbicides by TiO_2 aqueous suspension, J. Photochem. Photobiol. A: Chem. 159 (2003) 71–79.
[53] N. Guettaı, H.A. Amar, Photocatalytic oxidation of methyl orange in presence of titanium dioxide in aqueous suspension. Part II: Kinetics study, Desalination 185 (2005) 439–448.
[54] H. Scott Fogler, Elements of Chemical Reaction Engineering, fourth ed., PHI Learning Private Limited., New Delhi-110001, 2011.
[55] D. Chen, A.K. Ray, Photocatalytic kinetics of phenol and its derivatives over UV irradiated TiO_2, Appl. Catal. B: Environ. 23 (1999) 143–157.